Two kinesins drive anterograde neuropeptide transport

Angeline Lim*, Andreas Rechtsteiner, and William M. Saxton
Department of Molecular, Cell, and Developmental Biology, University of California, Santa Cruz, Santa Cruz, CA 95064

ABSTRACT **Motor-dependent anterograde transport, a process that moves cytoplasmic components from sites of biosynthesis to sites of use within cells, is crucial in neurons with long axons. Evidence has emerged that multiple anterograde kinesins can contribute to some transport processes. To test the multi-kinesin possibility for a single vesicle type, we studied the functional relationships of axonal kinesins to dense core vesicles (DCVs) that were filled with a GFP-tagged neuropeptide in the *Drosophila* nervous system. Past work showed that Unc-104 (a kinesin-3) is a key anterograde DCV motor. Here we show that anterograde DCV transport requires the well-known mitochondrial motor Khc (kinesin-1). Our results indicate that this influence is direct. Khc mutations had specific effects on anterograde run parameters, neuron-specific inhibition of mitochondrial transport by Milton RNA interference had no influence on anterograde DCV runs, and detailed colocalization analysis by superresolution microscopy revealed that Unc-104 and Khc coassociate with individual DCVs. DCV distribution analysis in peptidergic neurons suggest the two kinesins have compartment specific influences. We suggest a mechanism in which Unc-104 is particularly important for moving DCVs from cell bodies into axons, and then Unc-104 and kinesin-1 function together to support fast, highly processive runs toward axon terminals.**

Monitoring Editor
Gero Steinberg
University of Exeter

Received: Dec 8, 2016
Revised: Aug 16, 2017
Accepted: Sep 8, 2017

INTRODUCTION

Eukaryotic cells use cytoskeletal filaments and associated proteins to optimize the positions of their organelles. Neurons are particularly dependent on long-distance transport to maintain such cytoplasmic ordering, because of their asymmetry, length, and polar organization. Much of the biosynthesis of new neuronal components occurs in the cell body near the nucleus. However, the cell body usually contains less than 1% of the total cell volume. With most of the remaining cytoplasm contained in an elongated axon, the demand for transport of new components away from the cell body (anterograde) and a reciprocal return of spent components (retrograde) is intense (Saxton and Hollenbeck, 2012). Defining the machinery that drives transport and its regulation is an essential part of understanding how eukaryotic cells work. It is also a key part of understanding human neurodegenerative diseases such as hereditary spastic paraplegia, Charcot-Marie-Tooth disease, and amyotrophic lateral sclerosis that can be caused by defective transport (Goizet *et al.*, 2009; Crimella *et al.*, 2011).

The mechanism of long distance cytoplasmic movement relies on force generation by motor proteins that walk along microtubules. In axons, microtubules are oriented with their plus-ends distal toward the synaptic terminals (Heidemann *et al.*, 1981; Stone *et al.*, 2008; Janke and Kneussel, 2010). Plus-end directed kinesin motors drive anterograde transport, while minus-end directed cytoplasmic dynein motors drive retrograde transport. There are many types of plus-end directed kinesins. They have microtubule binding ATPase "motor" domains at the N-terminal that have different mechanochemical properties, in terms of speed and processivity of movement. Toward the C-terminal, anterograde kinesins have divergent "stalk-tail" domains that mediate linkage to cargoes, suggesting that different kinesins transport different sets of cytoplasmic components (Goldstein, 2001; Karcher *et al.*, 2002; Vale, 2003). Thus, identifying specific motor-cargo functional relationships is a central part of understanding how neurons and other

This article was published online ahead of print in MBoC in Press (http://www.molbiolcell.org/cgi/doi/10.1091/mbc.E16-12-0820) on September 13, 2017.

*Address correspondence to: Angeline Lim (angellim@ucsc.edu).

Abbreviations used: ANF, atrial natriuretic factor; CCAP, crustacean cardioactive peptide; DCV, dense core vesicles.

eukaryotic cells create and maintain optimal distributions of their cytoplasmic components.

Models of axonal transport for individual types of organelles have largely focused on one anterograde kinesin type. However, some transport mechanisms can employ more than one kinesin type (Hendricks *et al.*, 2010; Guardia *et al.*, 2016; Kulkarni *et al.*, 2017). For example, in *Drosophila* axons, there is evidence that kinesin-1 and kinesin-2 both influence the transport and distribution of acetylcholine (ACh) esterase vesicles (Kulkarni *et al.*, 2017). In HeLa cells; kinesin-1 appears to move lysosomes along perinuclear microtubules while kinesin-3 moves them along peripheral microtubules (Guardia *et al.*, 2016). In *Xenopus* oocytes, kinesin-1 and kinesin-2 can both bind VLE mRNPs and have overlapping functions in their cortical localization (Messitt *et al.*, 2008). In *Caenorhabditis elegans* sensory cilia, the highly processive movement of protein particles to the distal axoneme by intraflagellar transport is driven by the combined function of two different kinesin-2 motors at velocities intermediate between the intrinsic velocities of the two motors (Snow *et al.*, 2004). These observations suggest that different anterograde transport mechanisms may accomplish specific cargo distributions and delivery dynamics by employing multiple kinesins that have distinct biophysical properties.

Neuropeptides, synthesized and packaged into large dense core vesicles (DCVs) DCVs in the neuronal cell body, are transported anterograde to the nerve terminal for release (Kim *et al.*, 2006). Past work in *C. elegans*, *Drosophila*, and rat hippocampal neurons indicate that DCVs are carried anterograde by kinesin-3 (Zahn *et al.*, 2004; Pack-Chung *et al.*, 2007; Barkus *et al.*, 2008; Lo *et al.*, 2011). However, function disruptions of kinesin-3 do not completely inhibit anterograde DCV movement, and kinesin-1 has been implicated in distribution of the BDNF neuropeptide (Butowt and von Bartheld, 2007; Dompierre *et al.*, 2007). To address the possibility that DCVs employ a multi-kinesin anterograde transport mechanism we studied kinesins-1 and -3 influences on and associations with DCVs loaded with a GFP-tagged neuropeptide in *Drosophila* nervous systems using genetics, fluorescence microscopy, and superresolution colocalization analysis. The results indicate that kinesins-1 and -3 each have strong direct influences on DCV movement and that individual DCVs simultaneously bind both motors, indicating a dual kinesin anterograde transport mechanism.

RESULTS

Two kinesins are required for DCV transport

To determine whether DCV transport in *Drosophila* is driven by multiple members of the kinesin family, we first used neuron-focused RNA interference (RNAi) in *Drosophila* larvae to test three axonal kinesins. Neuronal RNAi of Unc-104 (a kinesin-3) caused general paralysis and lethality during the first instar. This is consistent with the effects of zygotic *Unc-104* null mutations (Zahn *et al.*, 2004; Pack-Chung *et al.*, 2007; Barkus *et al.*, 2008). Neuronal RNAi of Klp64D (a kinesin-2) caused no observable defects in behavior or development. Neuronal RNAi of Khc (classic kinesin-1) caused posterior paralysis followed by lethality in the third instar or pupal stages, similarly to the effects of strong zygotic *Khc* mutations (Saxton *et al.*, 1991; Brendza *et al.*, 1999). These results show that *Drosophila* larval neurons have cell-autonomous needs for both Unc-104 and Khc.

To test the possibility that Unc-104 and Khc have redundant roles in neurons, Khc was overexpressed in Unc-104 RNAi animals. Two different transgenic constructs that completely rescue homozygous *Khc* null mutants did not shift the early larval paralysis or lethality caused by Unc-104 knockdown in motor neurons. Furthermore, animals doubly heterozygous for null alleles of *Unc-104* and *Khc* showed no synthetic paralytic or lethal phenotypes. These results suggest that kinesin-1 and -3 functions in neurons are not redundant.

To determine whether kinesin-1 influences DCV transport, the distribution and movements of ANF::GFP, a neuropeptide fusion protein targeted to *Drosophila* DCVs (Rao *et al.*, 2001), was studied in larvae that carried a well-characterized *Khc* partial loss-of-function point mutation, either Khc^{6} (R741Q in Coil 2 of the stalk) or Khc^{17} (S246F in Loop 11 of the motor domain), over a null (Khc^{27}: Q65Stop in Helix 1 of the motor domain) (Brendza *et al.*, 1999). In the segmental nerves of fixed dissected mutants, ANF::GFP was concentrated in large focal accumulations (Figure 1A), which are a common consequence of *Khc* mutations (Gho *et al.*, 1992; Hurd *et al.*, 1996). ANF::GFP was greatly diminished at its normal location in synaptic terminal boutons (Figure 1, B and B′). Thus the proper distribution of DCVs in neurons is dependent on kinesin-1.

To observe the influences of Khc on general DCV motion, ANF::GFP was imaged in the axons of intact anesthetized larvae by time-lapse confocal microscopy. In live mutant nerves, DCVs were again seen in focal accumulations, and the number of DCVs undergoing long-distance movement in regions free of accumulations was greatly reduced (Figure 1C and Supplemental Movie 1). In Khc^{6}/Khc^{27} axons, we observed a sixfold reduction in anterograde flux and a 14-fold reduction in retrograde flux (Figure 1, C and D, and Table 1). Khc^{17}/Khc^{27} axons showed respective 2-fold and 6-fold reductions in flux. The changes in DCV distribution and the anterograde flux decreases are consistent with a role for kinesin-1 in anterograde DCV transport. The retrograde flux decreases likely reflect two things: that any DCVs carried by retrograde transport must first be delivered to distal regions by anterograde transport and that anterograde and retrograde microtubule motor functions are interdependent in many transport processes (Brady *et al.*, 1990; Martin *et al.*, 1999; Ling *et al.*, 2004; Pilling *et al.*, 2006; Barkus *et al.*, 2008; Uchida *et al.*, 2009; Encalada *et al.*, 2011).

Anterograde DCV transport is not influenced by axonal mitochondria distribution

Kinesin-1 is an anterograde motor for axonal mitochondria (Saxton and Hollenbeck, 2012; Maday *et al.*, 2014). *Khc* mutations stop most mitochondrial movement and thus may compromise local aerobic ATP-production and other mitochondrial functions in axons (Pilling *et al.*, 2006). Since the established DCV motor, Unc-104, uses ATP hydrolysis to drive transport, the negative effects of *Khc* mutations on DCVs might be indirect through depression of axonal ATP levels. To test this possibility, we studied DCV transport in axons depleted of mitochondria by neuronal RNAi of Milton, a specific Khc-mitochondria linker protein (Stowers *et al.*, 2002; Glater *et al.*, 2006). Milton RNAi in motor neurons severely reduced the number of mitochondria present in segmental nerve axons (Figure 2A), consistent with phenotypes caused by zygotic *Milton* mutations (Glater *et al.*, 2006). Mitochondrial-GFP signal was intense in the ventral ganglion, where motor neuron cell bodies are located. Close to the ventral ganglion and in axons traversing the anterior larval segments (A3–A4), some mitochondria could be seen, but they were largely stationary (Figure 2B and Supplemental Movie 2). In more distal portions of axons (beyond A4) no mitochondria were detected.

To study the influence of this depletion on DCV transport, ANF::GFP was coexpressed in motor neurons with Milton inhibitory RNA. Surprisingly, live animals had focal accumulations of DCVs

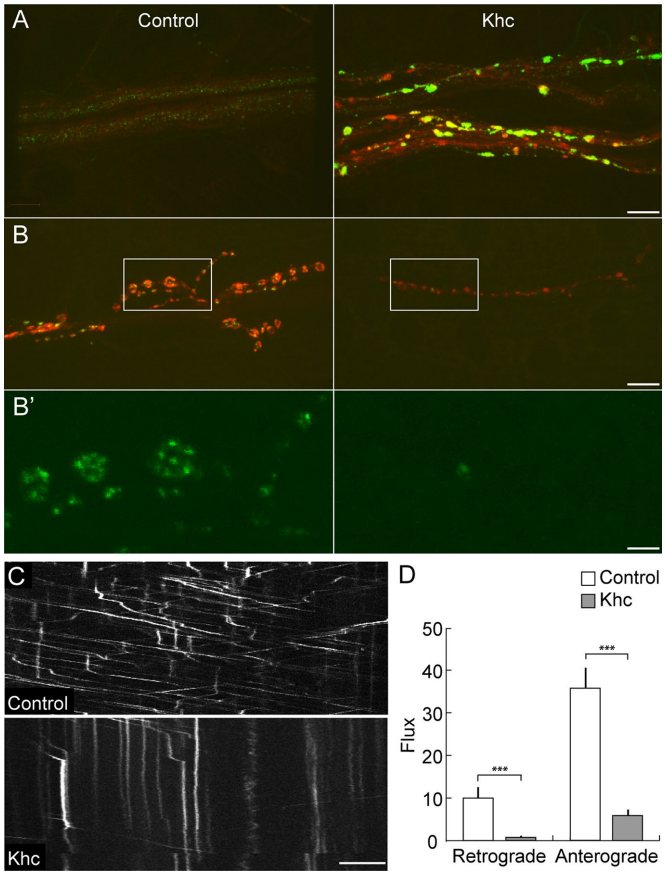

FIGURE 1: Kinesin-1 influences the distribution and flux of axonal DCVs. A Gal4-UAS controlled ANF::GFP that concentrates in DCVs was expressed in neurons of control and *Khc* mutant (*Khc*^{6}/*Khc*^{27}) larvae using the *P{GawB}D42* Gal4 driver. (A) Confocal images of fixed control and *Khc* mutant segmental nerves passing through segments A4–A5 showing distributions of ANF::GFP (green) and an antibody to CSP (red), which is a vesicle associated synaptic protein. In this and subsequent figures, the ventral ganglion (motor neuron cell bodies) is to the left. Note the shift from a finely punctate GFP signal in control nerves to large focal accumulations of signal in the mutant axons (scale bar = 12 µm). (B) Synaptic terminals on muscles 6 and 7 of control and *Khc* mutant larvae in segments A4–A5 (scale bar = 12 µm). (B′) Higher magnification of the boxed areas in B showing the DCV signal alone (scale bar = 3 µm). Note the scarcity of DCVs in the *Khc* mutant boutons. (C) Kymographs of ANF::GFP signal created from 100 s time-lapse image series (2 frames/s) of a control or a *Khc* mutant segmental nerve. Each kymograph shows DCV positions (*x*-axis, bar = 5 µm) as a function of time (*y*-axis, time = 0 s at top). Negative slopes, positive slopes, and vertical lines show anterograde, retrograde, and stationary DCVs, respectively. (D) Quantification of DCV flux (number of DCVs observed moving past a perpendicular line in a segmental nerve per minute). Bars show mean ± SE for $n = 10$ animals per genotype (one nerve per animal). Brackets show significant differences between *Khc* mutant and control values as determined by a Student's *t* test (***$p \leq 0.001$).

along their segmental nerves (Figure 2C), especially in distal regions. This was unexpected, because in tests that have focused on GFP-mitochondria distribution in *Milton* mutants (Figure 2A; Hall and Hedgecock, 1991; Pack-Chung *et al.*, 2007), focal accumulations of mitochondria were not evident. The DCV focal accumulations indicate that acute Milton inhibition indeed causes axonal swellings in which transported organelles can accumulate. However, in regions without swellings, anterograde DCV transport appeared normal, even in distal segments that completely lacked axonal mitochondria (Figure 2, D and E, and Supplemental Movie 3). This suggests that DCV transport inhibition caused by *Khc* mutations is due neither to the depletion of axonal mitochondria nor to steric blockade of DCV passage by axonal swellings.

Association of both kinesins with individual DCVs

If kinesin-1 is a motor for DCVs, then it must associate with them. As an initial test, we looked for motor-DCV cofractionation through differential and sucrose gradient sedimentation of homogenates generated from flies expressing ANF::GFP in neurons. Western blots showed that Khc was elevated in fractions that contained ANF::GFP, as was Unc-104. Cytochrome C staining showed that the Khc in those fractions was not due to the presence of mitochondria. However, Rab 11 staining suggested that organelles other than DCVs were also present in those fractions (Supplemental Figure S1).

To test more directly for motor association with DCVs, we used fluorescence microscopy to study cells cultured from ventral ganglia of larvae that expressed ANF::GFP in motor neurons. Time-lapse imaging of live cells showed that most DCV transport, even in neurites, was short range and saltatory, but some did make long movements (Supplemental Figure S2). The simple optical path provided by the cultured neurons allowed high-resolution immunolocalization of motors and DCVs by superresolution microscopy. Stacks of optical sections were used to generate three-dimensional (3D) reconstructions of ANF::GFP, anti-Khc, and anti-Unc-104 distributions (Figure 3). For analysis of motor–DCV association, object-based colocalization was used (Lachmanovich *et al.*, 2003). A spacing threshold between of 180 nm was selected for defining colocalization of motor and DCV centroids, based on initial testing and the sizes of DCVs, motors, and IgG (Roux *et al.*, 1998; Al-Bassam *et al.*, 2003; Jeppesen and Hoerber, 2012). Detailed analysis of all DCV signals in six cells from three independent experiments showed colocalization of anti-Khc and anti-Unc-104 with 26.9 ± 2.3% and 29.2 ± 2.8%, respectively, of ANF::GFP punctae. Simultaneous colocalization of both motors was seen with 15.2 ± 1.8% of ANF::GFP punctae. This is ~twofold greater than the simple 8.3% predicted by chance (Chitest, *p* value < 0.001) (Figure 3C).

To test motor–DCV colocalization more rigorously, we compared the observed colocalizations to expected colocalizations if Khc and Unc-104 were not associated with DCVs but were localized randomly. We simulated random locations for Khc or Unc-104 punctae in one region of interest (ROI) per cell body. Expected random colocalizations between the random motor locations and the positions of real DCV punctae was then calculated with threshold distances ranging from 100 to 700 nm. The derived expected random colocalization frequencies were significantly less than the observed colocalization frequencies in the same ROI at threshold distances of less than 400 nm (Figure 3D). The fold difference (observed/random) ranged from sevenfold at 140 nm to twofold at 300 nm (Figure 3E). This indicates that dual kinesin colocalization with DCVs in cultured motor neurons is nonrandom, suggesting a mechanism of DCV transport that can employ both kinesins on the same organelle.

Kinesin-1 and -3 contributions to axonal DCV motion

To look for influences of the two kinesins on DCV transport, we quantified DCV run behaviors in motor axons of live larvae by single organelle tracking. If kinesin-1 and -3 function separately, either

Genotype	# Larvae (# runs)	Flux (DCV/min)	Run length (μm)	Run velocity (μm/s)	Duty cycle	
					Fwd run (%)	Pause (%)
Anterograde						
Control	10 (95)	35.7 ± 4.6	19.1 ± 4.7	0.96 ± 0.10	94.0 ± 3.5	5.0 ± 3.2
Khc^{6}/Khc^{27}	10 (174)	5.9 ± 1.3***	6.2 ± 2.1***	0.67 ± 0.09***	85.0 ± 5.7**	15.0 ± 5.4**
Khc^{17}/Khc^{27}	10 (182)	16.5 ± 2.0***	10.4 ± 3.7***	0.80 ± 0.11***	86.0 ± 5.1**	14.0 ± 5.1**
Retrograde						
Control	10 (161)	10.1 ± 2.5	–8.0 ± 2.3	–0.97 ± 0.10	87.0 ± 3.8	11 ± 3.2
Khc^{6}/Khc^{27}	10 (50)	0.7 ± 0.2***	–5.5 ± 1.5	–0.85 ± 0.11	80.0 ± 8.9	18 ± 7.9
Khc^{17}/Khc^{27}	10 (94)	1.6 ± 0.6***	–9.7 ± 3.7	–1.00 ± 0.11	80.0 ± 7.3*	15 ± 5.4

ANF::GFP loaded DCVs in segmental nerve axons of live larvae were individually tracked and behaviors were quantified. All values represent mean ±SE. Comparisons of mutant to control flux values were done using a Student's t-test. Linear contrast was used for all other comparisons. P-values are indicated by asterisks (* <0.05, ** ≤0.01, *** ≤0.001). The genotype of Khc mutant animals was Khc^{6} or $^{17}/Khc^{27}$; *P[GawB]D42*, *P[w^{+mC} UAS-ANFGFP]3*/+. The control genotype was *P[GawB]D42*, *P[w^{+mC} UAS-ANFGFP]3*/+.

TABLE 1: Effects of *Khc* mutations on DCV transport in axons.

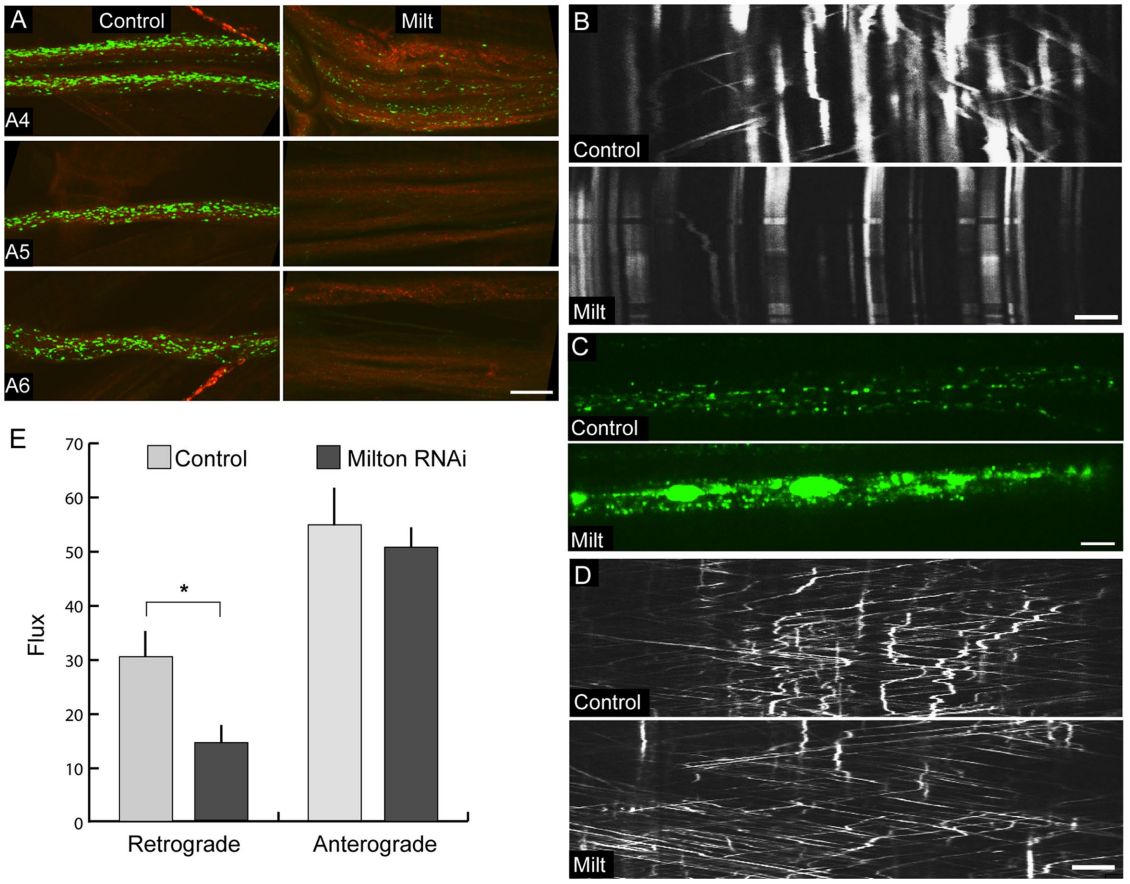

FIGURE 2: Axonal mitochondria depletion by Milton knockdown does not alter anterograde DCV transport. Expression of a Milton shRNAi transgene was induced in motor neurons of animals along with either mito-GFP or ANF::GFP, using the OK^{371}-GAL4 driver. (A) Confocal images of fixed segmental nerves in control and Milton RNAi (Milt) larvae showing mitochondrial-GFP with enhanced sensitivity using anti-GFP (green) and anti-CSP (red) (scale bar = 20 μm). Note that, even with the anti-GFP enhancement, axonal mitochondria were not observed in distal axon regions (A5–A8) of Milton RNAi larvae. (B) Kymographs of time-lapse image series in more proximal segments (A2–A3) where more mitochondria were present show that Milton RNAi inhibited most mitochondria transport in motor axons (*x*-axis bar = 5 μm; *y*-axis *t* = 0 s at top and 100 s at bottom; 1 frame/s). (C, D) Confocal images of ANF::GFP loaded DCVs in motor axons of live larvae. (C) Single frames showing large swellings that contain DCVs in Milton RNAi motor axons (scale bar = 5 μm). (D) Kymographs of ANF::GFP in swelling-free portions of distal motor axons (A5–A6) show that Milton knockdown had little effect on DCV motion (*x*-axis bar = 5 μm; *y*-axis *t* = 0 s at top and 100 s at bottom; two frames/s). (E) Quantification of ANF::GFP DCV flux in control (*n* = 6) and Milton RNAi (*n* = 8) larvae (1 nerve per animal) in segments A5–A6. Bars show mean ± SE. Retrograde DCV flux was somewhat reduced, but anterograde flux was not affected (*$p \leq 0.05$).

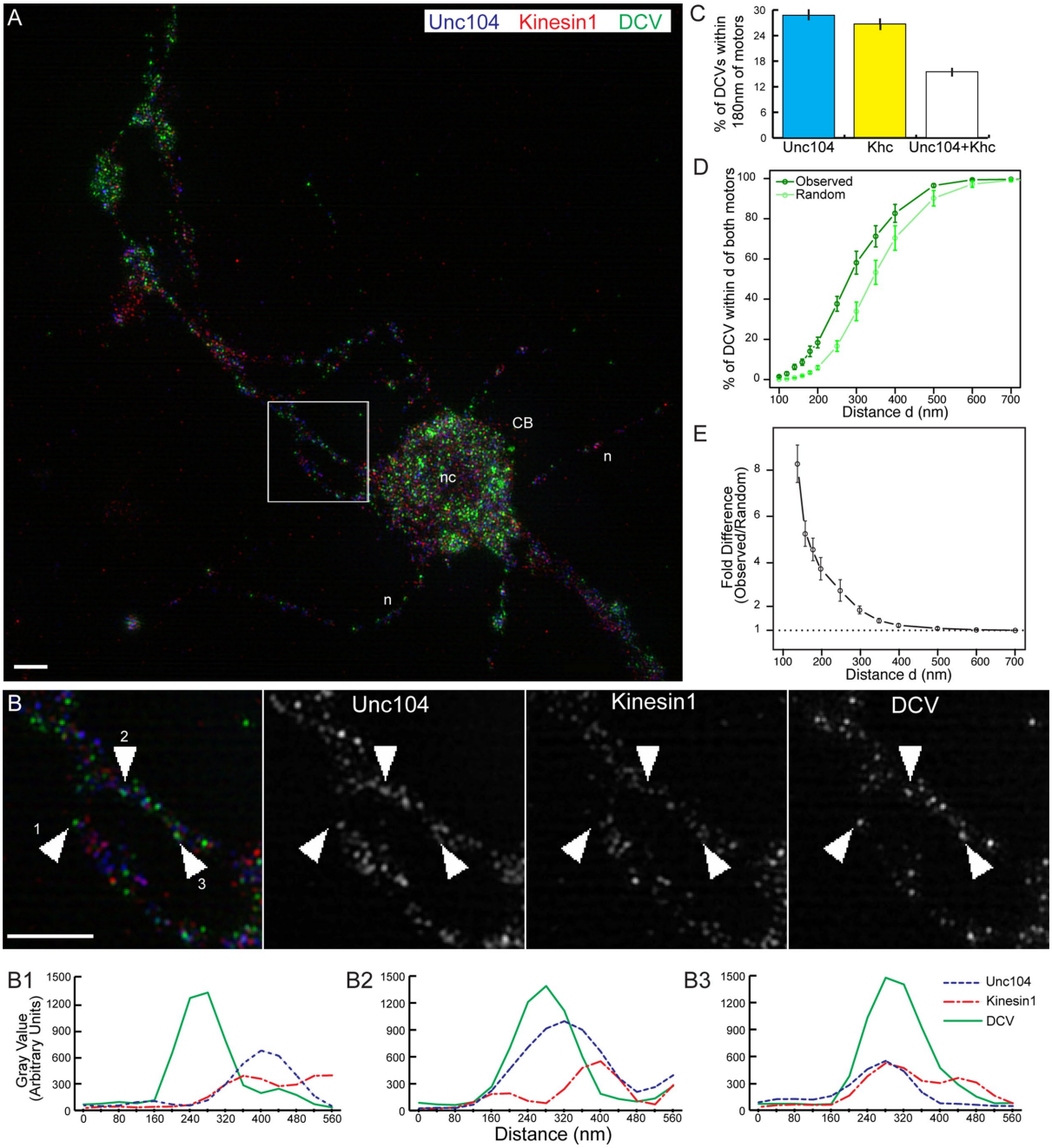

FIGURE 3: Unc104 and kinesin-1 colocalize with DCVs in neurons. Primary neurons were cultured from larvae that expressed ANF::GFP in motor neurons (OK^{371} driver). (A) A maximum projection of a 3D SIM superresolution Z-series of a motor neuron with ANF::GFP/DCVs (green) stained with anti-Unc104 for kinesin-3 (blue) and anti-Khc for kinesin-1(red). The neuron had neurites (n) growing out of the cell body (CB). The nucleus (nc) was identified by DAPI staining (not shown). (B) An expanded view of the box marked in A. Arrowheads (1–3) point to DCVs whose centroids are within 180 nm of anti-Khc and anti-Unc-104 centroids. Scale bars in A and B = 2 μm. (B1–B3) Line scans across the three marked DCVs and motor punctae show fluorescence intensities as a function of position. (C) The mean percentage (±SE) of DCV punctae that were within 180 nm of anti-Unc104, anti-Khc, or both as measured in three dimensions from Z-stacks of entire cells ($n = 6$ cells from three different experiments). Note that the fraction of DCVs that colocalize with both motors (15.2%) is nearly twofold greater than predicted by chance (8.3%). (D) To assess differences between observed and chance colocalization over a range of threshold distances, Khc and Unc104 locations were randomly and uniformly distributed across a volume region of interest (ROIs) within each of the six cells. This was repeated 100 times for each ROI. A mean colocalization (±SE) of real DCV punctae with the random motor punctae was then determined for each iteration at a variety of distance thresholds for each of the six ROIs (random). Colocalization of DCVs with real motor signals in the same ROIs was determined over the same range of threshold distances (observed). At 400 nm and less, the observed vs. random values were significantly different (Chitest, p value ≤ 0.001) (E) Plot showing the mean (±SE) of the fold differences between observed and random colocalization across the six ROI analyzed for D as a function of threshold distance.

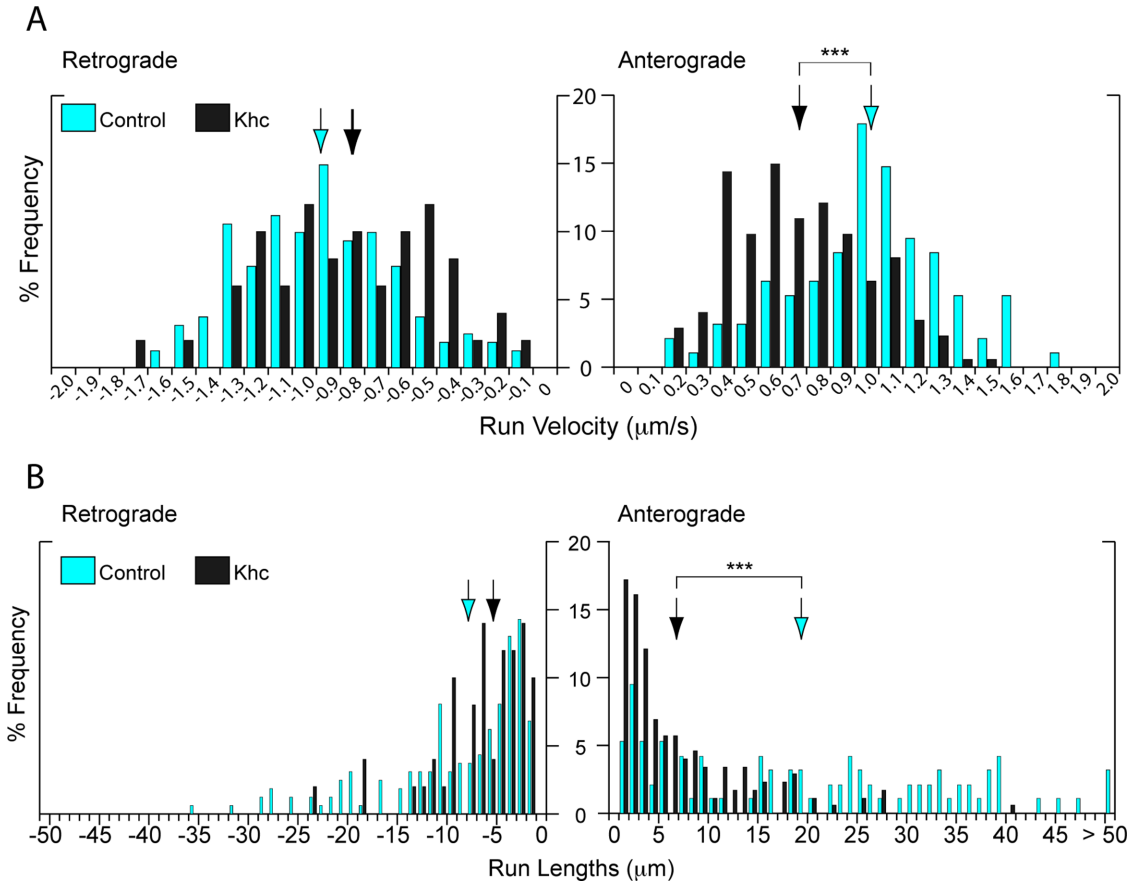

FIGURE 4: Kinesin-1 influences on DCV runs. Mobile DCVs were individually tracked, and their run behaviors were quantified in control and *Khc* mutant larval axons. The mutant data displayed were collected from Khc^{6}/Khc^{27} animals. (A) Frequency distributions for run velocities (bin size = 0.1 μm/s). Arrows indicate means for each distribution. Note the single mode distribution of anterograde run velocities and the shift toward slower velocities in Khc mutants (right panel). (B) Frequency distributions for run lengths (bin size = 1 μm). Arrows indicate means for each distribution. Note the shift toward shorter anterograde run lengths in *Khc* mutants (right panel). ***$p < 0.001$.

on different sets of DCVs or in distinct runs when together on a single vesicle, then the intrinsic velocity differences determined for Khc and Unc-104 in vitro (0.5–0.8 and 2 and 3 μm/s, respectively) might be reflected in distinct sets of DCV run velocities (Klopfenstein *et al.*, 2002; Tomishige *et al.*, 2002; Snow *et al.*, 2004). No evidence of this was found (Figure 4A and Table 1). Anterograde run velocities were broadly distributed but fell into a single mode with a mean of 1 μm/s, intermediate between the in vitro velocities.

To test the possibility that the single run velocity mode simply reflects a wide overlap of in vivo velocities for the two motors, the influences of *Khc* mutations were analyzed. If kinesins-1 and -3 make independent contributions, then reduced Khc function should skew the distribution toward higher kinesin-3 run velocities. However, anterograde DCV-run velocity actually decreased significantly in *Khc* mutant axons (Figure 4A and Table 1), arguing against a simple mixture of independent single-motor runs.

One of the striking features of anterograde DCV transport was run length. In wild-type axons, pauses were rare, so DCVs often traversed the entire field of view in a single run (Figure 1C). Simply using the first and/or last positions at which organelles were visible at the edge of the field of view as endpoints, the average length of all observed anterograde runs was 19.1 ± 1.5 μm. To estimate an actual run length that avoids clipping by the field of view, the total of all DCV anterograde run lengths (1869 μm) was divided by the total number of pauses observed (61). This predicts an average run length of 83 μm. Khc^{6}/Khc^{27} mutants showed a threefold decrease in DCV run length relative to the 19 μm measured mean (Figure 4B and Table 1) and a 13-fold decrease relative to the 83 μm estimated mean. Our past work in the same system showed that *unc-104* mutations cause anterograde run parameter decreases of a similar magnitude (Barkus *et al.*, 2008). Overall, the effects of the *Khc* and *unc-104* mutations indicate that both kinesins make important positive contributions to anterograde DCV run velocity and length.

Comparison of the effects of *Khc* and *unc-104* mutations on retrograde DCVs showed interesting contrasts. Retrograde run velocities and lengths are reduced substantially by *unc-104* mutations (Barkus *et al.*, 2008) but were not significantly affected by *Khc* mutations (Figure 4 and Tables 1 and 2). This lack of an observable influence of Khc on retrograde runs provides two important insights. First, axonal swellings and pleiotropic physiological changes caused by Khc mutations do not cause steric hindrance or other nonspecific defects in DCV transport along microtubules. Second, Unc-104 has an important functional relationship with the retrograde DCV transport machinery.

To investigate the general assumption that cytoplasmic dynein is the primary retrograde motor for all axonal organelles, we conducted

	Kinesin-1	Kinesin-3
Anterograde DCVs		
Flux	31%	27%
Run length	43%	50%
Run velocity	77%	53%
Retrograde DCVs		
Flux	11%	57%
Run length	95%	46%
Run velocity	95%	67%

DCV flux, run length, and run velocity expressed as a percentage of control values. Averages are shown of values from tw different allelic combinations for kinesin-1 (Khc^{6}/Khc^{27} and Khc^{17}/Khc^{27}) (presented here) and for kinesin-3 ($unc\text{-}104^{O1.2}/ unc\text{-}104^{P350}$ and $unc\text{-}104^{O3.1}/ unc\text{-}104^{P350}$) (Barkus *et al.*, 2008).

TABLE 2: Comparison of DCV transport parameters in kinesin-1 and kinesin-3 mutants.

a full analysis of the effects of *Dhc64C* mutations on DCV behavior in live animals (Supplemental Table 1 and Supplemental Figure S3). They caused substantial and significant reductions in retrograde DCV flux, run length, and run velocity, suggesting that indeed cytoplasmic dynein is the retrograde DCV motor. Anterograde runs were compromised somewhat less, consistent with prior observations on anterograde-retrograde transport interdependence (Brady *et al.*, 1990; Martin *et al.*, 1999; Ling *et al.*, 2004; Pilling *et al.*, 2006; Barkus *et al.*, 2008; Uchida *et al.*, 2009; Encalada *et al.*, 2011). Taken together, our analyses of axonal DCV motion indicate that kinesin-1 and kinesin-3 make equivalent important contributions to the anterograde transport mechanism and that kinesin-3 makes positive contributions to the dynein-dependent retrograde transport mechanism.

Different influences of kinesin-1 and -3 along a peptidergic neuron transport path

Based on evidence that zygotic *unc-104* mutant embryos retain small transport vesicles in neuronal cell bodies and have few vesicles in axons, along with evidence that other kinesins could contribute to anterograde vesicle transport, it has been suggested that kinesin-3 carries small vesicles from cell bodies into axons where other kinesins drive long-distance transport toward synaptic terminals (Pack-Chung *et al.*, 2007; Goldstein *et al.*, 2008). To investigate this possibility for large DCVs, we analyzed the effects of cell-specific RNAi knockdown of Khc or Unc-104 on the distribution of ANF::GFP in and near the cell bodies of peptidergic neurons using the CCAP-Gal4 driver (Ewer *et al.*, 1994; Park *et al.*, 2003) (Figure 5). The locations of those neurons deep within the ventral ganglion did not allow high-quality live imaging, so an immunostaining approach was used on dissected larval neuromuscular preparations. In controls, punctate ANF::GFP signals were abundant in CCAP cell bodies (Figure 5, B and E, arrows) and were well dispersed along their neurites (Figure 5H, arrowheads). CCAP cell bodies project their primary neurites toward the midline of the ventral ganglion where they arborize (Figure 5H, asterisk). ANF::GFP signal was detected there at the midline and in the longitudinal tracts that are composed of bundles of dendrites and axons (Figure 5H, "LT"). In CCAP motor axons that project away from the ventral ganglion in segmental nerves, signal was distributed in a fairly even punctate pattern (Figure 5K).

DCV distributions in CCAP neurons subjected to Khc and Unc-104 RNAi showed interesting differences. Unc-104 knockdown resulted in intense DCV accumulation in cell bodies (Figure 5F), reduced levels in primary neurites (Figure 5I, inset), and almost eliminated DCVs more distally: including at midline arbors, in longitudinal tracts, and in motor axons (Figure 5, I and L). In comparison, Khc knockdown caused a less-intense accumulation of DCVs in cell bodies (Figure 5G), allowed a relatively normal DCV distribution in primary neurites (Figure 5J, inset), and caused a strong overaccumulation of DCVs at the midline zone of arborization (Figure 5J, asterisk). In motor axons, DCV signal was abundant, but much of it was in clusters or large focal accumulations (Figure 5M). These results suggest that kinesin-3 is particularly important for DCV exit from the cell body, that kinesin-1 is particularly important for normal transport along axons, and that kinesin-1 has some special role in preventing DCV accumulation in the midline arborization zone.

DISCUSSION

Defining transport mechanisms that are used to establish and maintain proper distributions of subcellular components is of great importance for understanding how cells work and for understanding the pathologies of transport related human diseases. The discovery of cytoskeletal motor protein superfamilies, particularly the kinesin superfamily, revealed a great potential for diversity of transport mechanisms and brought into focus the importance of research into the specifics of how different subcellular components are moved (Goldstein, 1991). Subsequent work has shown that cargo-specific mechanisms are indeed diverse. Excellent advances have been made for some cargoes, but major gaps remain for many (Maday *et al.*, 2014). The studies presented here address the question of which microtubule motors move DCVs that carry a specific neuropeptide. Our results show that proper DCV transport and distribution in neurons requires two different anterograde motors, classic Khc-driven kinesin-1 and an Unc-104-driven kinesin-3.

Our previous model for DCV transport in *Drosophila* neurons centered on force generation by Unc-104 (Pack-Chung *et al.*, 2007; Barkus *et al.*, 2008), so the requirement for Khc identified in our initial tests raised questions about whether its role is direct. Our subsequent results are consistent with both Khc and Unc-104 serving directly as anterograde DCV motors. First, neuron-specific knockdown of Khc or Unc-104 caused cell-autonomous defects in DCV transport and distribution, so pleiotropic effects from Unc-104 malfunction in the whole animal are unlikely to be an issue. Second, we tested for indirect effects on DCV transport that might be due to disrupted Khc-driven transport of neuronal mitochondria. Neuron-specific knockdown of the Khc-mitochondria attachment factor Milton did not cause defects in anterograde DCV transport in distal axons, despite an absence of mitochondria. The robust DCV transport is especially interesting in light of the fact that Milton knockdown caused the sort of focal accumulations of fast transport materials that occur in axonal swellings in *Khc* mutants (Gho *et al.*, 1992; Hurd *et al.*, 1996), suggesting that DCV transport/distribution problems in *Khc* mutants are not due to "traffic jam" type steric hindrance. Third, the frequency of Khc and Unc-104 colocalization with DCVs, when quantified by superresolution microscopy, ranged from sevenfold greater than random within a tight radius (140 nm) to twofold greater than random within a loose radius (400 nm) and random at greater threshold distances. This suggests that individual DCVs can simultaneously bind both kinesins. Finally, single organelle tracking analysis showed that *Khc* mutations cause significant and substantial reductions in anterograde DCV run parameters; effects equivalent to those caused by *Unc-104* mutations. Taken

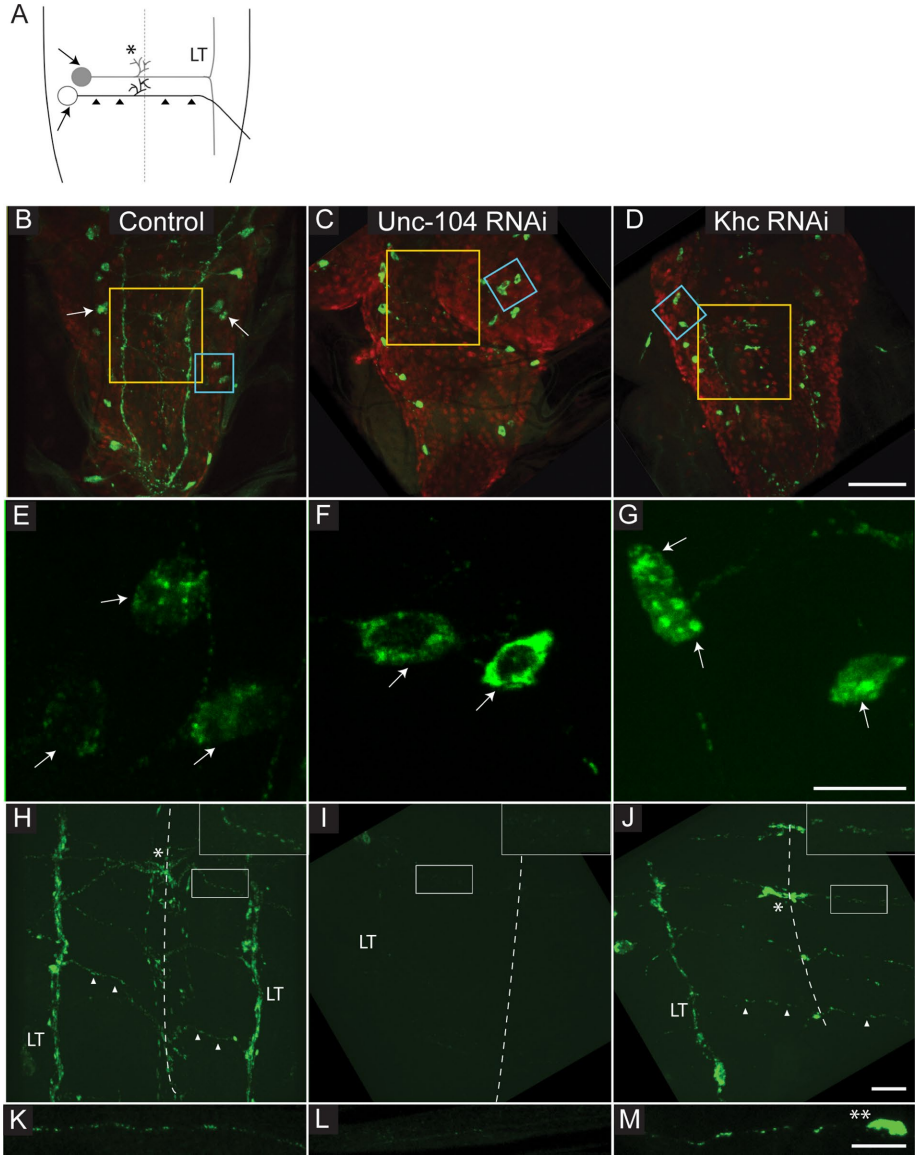

FIGURE 5: Kinesin-1 and kinesin-3 have different effects on DCV distribution in neurons. CCAP GAL4, which is expressed in four neurons per segment in A1–A4 of the ventral ganglion, was used to coexpress ANF::GFP (green) with either Khc RNAi or Unc-104 RNAi. Anti-elav was used to stain all neurons (red). (A) Diagram illustrating that the primary neurites of the two CCAP neurons (arrows) in each hemisegment extend toward the midline (dashed line) where they arborize (*). The axon of the motor neuron (white circle, black line) then proceeds across the contralateral longitudinal tract (LT) and leaves the ganglion in a segmental nerve, eventually synapsing with body wall muscles 12 and 13 (Hodge *et al.*, 2005; Vomel and Wegener, 2007). The neurite of the interneuron (black circle, gray line) projects to the contralateral tract and then bifurcates to project in both directions along it (LT) (Santos *et al.*, 2007; Vomel and Wegener, 2007; Karsai *et al.*, 2013). (B–D) Large-depth-of-field maximum projections of confocal Z-stacks of ANF::GFP DCVs (green) in CCAP neurons and of anti-Elav (red) in ventral ganglia of fixed larvae. The images in each column were collected with identical confocal and camera settings, so the differences in fluorescence intensities for different genotypes can be compared directly. Examples of CCAP neuron cell bodies are marked by arrows in B. The blue and yellow boxes mark areas with expanded views in E–G and H–J, respectively. Scale bar = 50 µm. (E–G) Expanded view of the blue boxes from B to D showing CCAP cell bodies (arrows). Scale bar = 10 µm. (E) Note the fairly even distribution of ANF-GFP punctae in the control cell body. (F) Unc-104 RNAi caused overaccumulation of ANF-GFP signal in cell bodies. This is seen in the cell body on the right, which was entirely within the Z-stack. The cell body on the left, which was only partially in the Z-stack, shows that the bright signal reflects crowding of punctae. DCVs in Unc-104 RNAi neurites were rare. (G) Khc RNAi caused some clumped accumulation of ANF-GFP in cell bodies. (H–J) Images of the central regions of the ventral ganglia (yellow boxes in B–D) giving views of neurites and longitudinal tracts. Insets show expanded views of the neurite commissures. Primary neurites (white arrowheads) project in commissures toward the midline (dashed line) where they arborize. Note that Unc-104 RNAi (I) greatly reduced DCV signal in neurites (inset), at the midline arborization zone, and in longitudinal tracts (LT). In contrast, Khc RNAi (J) showed strong DCV signal in longitudinal tracks and commissures, while causing excessive DCV signal in the arborization zone. Scale bar = 10 µm. (K–M) Images of DCVs in CCAP axons within segmental nerves as they leave the ventral ganglia. Note that DCVs are rarely seen in Unc-104 RNAi axons (L). They are present in the Khc RNAi axon (M) but are clustered and often appear in focal accumulations (**). Scale bars = 10 µm. These images are representative of five larvae analyzed for each genotype.

together, these results indicate that Khc is a motor for DCVs and that the importance of its contribution to the anterograde DCV transport mechanism is equivalent to that of Unc-104.

Why are two types of anterograde microtubule motors needed for DCV transport in neurons? One possibility derives from the fact that microtubules acquire posttranslational modifications over time and that kinesin-1 and kinesin-3 have preferences for different types of microtubules (Brown *et al.*, 1993; Cai *et al.*, 2009; Guardia *et al.*, 2016). Our differential effects in CCAP neurons of Khc and Unc-104 knockdowns on DCV distributions, with greater Unc-104 influences near the cell body and greater Khc influences in axons, could reflect different distributions of modified microtubules along the transport path. However, if differential microtubule modification distributions contribute to the DCV transport mechanism, the population of microtubules in axons must be mixed, because both motors have strong influences on anterograde DCV runs in axons.

Another possibility for a dual kinesin mechanism is that the physical challenges for proper DCV transport and distribution in axons require the combined output of both motors. In our system, axonal mitochondria move anterograde in short runs (avg. = 1.86 µm) at 0.26 µm/s, and maintain a fairly even distribution of mitochondria all along the axon, presumably to serve local metabolic and signaling needs (Saxton and Hollenbeck, 2012). Those anterograde runs appear to be driven solely by Khc with no significant contributions from Unc-104 (Pilling *et al.*, 2006; Barkus *et al.*, 2008). Axonal DCVs move anterograde in extremely long runs

(avg. = 83 μm) at 0.96 μm/s to concentrate at the terminal. Thus DCV runs in larval axons are 3-fold faster and a remarkable 45-fold longer than those of mitochondria. Perhaps a dual kinesin mechanism for DCVs facilitates exceptionally processive and fast anterograde runs. Kinesin-3 is a fast motor when dimerized, but its ability to form dimers is weak and individual monomers are not processive (Nangaku *et al.*, 1994; Klopfenstein *et al.*, 2002; Tomishige *et al.*, 2002; Norris *et al.*, 2014). Kinesin-1, although slower, is strongly dimerized and can be quite processive (Howard *et al.*, 1989; Block *et al.*, 1990). It may be that tenacious kinesin-1 interactions with microtubules, while contributing drag that reduces DCV velocity, help keep kinesin-3 dimerized, fully active, and engaged with the microtubule.

MATERIALS AND METHODS

Drosophila strains

Drosophila were cultured with 12hr light–dark cycles at 22–25°C, using standard protocols (http://flystocks.bio.indiana.edu/Fly_Work/media-recipes/bloomfood.htm). Except where noted otherwise, all fly strains were obtained from the Bloomington Stock Center (http://flystocks.bio.indiana.edu/). The transgenes *P{w^{+mC} UAS-GFPmito}AP.3*, which targets GFP to the mitochondria matrix (Pilling *et al.*, 2006), or *P[w^{+mC} UAS-ANFGFP]3*, which targets GFP to DCV lumens (Rao *et al.*, 2001), were expressed in neurons using a *P[GawB]D42* Gal4 "driver" or were expressed more specifically in motor neurons using *P[GawB]VGlut^{OK371}*. For biochemical fractionation, *P[w^{+mC} UAS-ANFGFP]3* was expressed using *P[tubP-GAL4]LL7*.

Kinesin-1 mutants were constructed by crossing hypomorphic missense alleles (*Khc^{6}, or Khc^{17}*) over a null (*Khc^{27}*) (Brendza *et al.*, 1999). For RNAi inhibitions, fly strains carrying Gal4-UAS controlled transgenes capable of expressing hairpin RNAs specific for Khc (*P{TRiP.GL00330}attP2*), for Klp64D (*P{TRiP.HMS02193}attP40*), for Unc-104 (*P{TRiP.HMC03512}attP40*), or for Milton (*P{TRiP.JF03022}attP2*) were obtained from the Transgenic RNAi Project (TriP; Harvard University, http://www.flyrnai.org/TRiP-HOME.html). To enhance the efficacy of Milton knockdown, Dicer (*P{w[+mC] = UAS-Dcr-2.D}1*) was coexpressed with the Milton RNAi construct. For DCV distribution studies in CCAP neurons, coexpression of RNAi constructs and ANF::GFP was enhanced by placing two CCAP-GAL4 drivers (*P{CCAP-GAL4.P}16* and *P{CCAP-GAL4.P}9*) in each animal. Because RNAi transgenes were expressed in only a subset of neurons (motor neurons or CCAP neurons) we were unable to measure the extent of gene knockdown with real time PCR (RT–PCR). However, all the RNAi lines used had phenotypes similar to well-characterized, published zygotic mutants. To test for rescue of lethality caused by Unc-104 RNAi in motor neurons driven by *P{GawB}VGlut^{OK371}*, two different Khc overexpression constructs were used. One is a genomic transgene that includes the native *Khc* locus and *cis*-regulatory elements (Saxton *et al.*, 1991). The other is a transgene with a ubiquitin promoter driving overexpression of a myc-tagged *Khc* cDNA (*P{w^{+},wumk9}*) created in Larry Goldstein's lab (deCuevas, 1993).

Fractionation of *Drosophila* cytoplasm and Western blotting

To fractionate DCVs, 2 g of adult flies with ANF::GFP expression driven by the *P{tubP-GAL4}LL7* driver were homogenized on ice using a mortar and pestle in 10 ml of homogenization buffer (250 mM sucrose, 100 mM K-acetate, 40 mM KCl, 20 mM HEPES, 10 mM Tris, 5 mM EGTA [ethylene glycol-bis(β-aminoethyl ether)-*N*,*N*,*N*′,*N*′-tetraacetic acid], 5 mM $MgCl_2$, 1 mM MgATP, 1 complete mini-EDTA free protease inhibitor tablet [Roche Diagnostics, Indianapolis, IN], pH 7.4). Despite the ubiquitous expression pattern of *P{tubP-GAL4}LL7* (O'Donnell *et al.*, 1994), GFP was detected only in the nervous system, suggesting that the ANF::GFP mRNA or protein is unstable in nonneuronal cells. To remove fly debris, homogenate was filtered through a nitex mesh (pore size = 140 μm) and then clarified by centrifugation twice at 1300 × *g* for 5 min. Most mitochondria were then eliminated by centrifugation for 10 min at 5000 × *g*. Postmitochondrial supernatants from two preparations were pooled and DCVs were pelleted by centrifugation at 100,000 × *g* for 20 min. The pellet was resuspended in 1 ml homogenization buffer, overlaid on a 20–60% sucrose gradient prepared on The Gradient Station (Biocomp Instruments), and centrifuged at 134,000 × *g* for 90 min in a swinging bucket rotor.

Fractions collected from the top of the gradient were analyzed by SDS–PAGE and Western blotting. After blocking in Tris-buffered saline (TBS)/Tween20 with 3% nonfat milk, blots were incubated with primary antibodies diluted in blocking solution: rabbit anti-Imac/Unc-104, 1:1000 (Pack-Chung *et al.*, 2007), rabbit anti-*Drosophila* Khc, 1:1000 (Cytoskeleton), mouse anti-GFP, 1:1000 (Clonetech), anti-rab11, 1:1000 (Dollar *et al.*, 2002), and mouse anti-cytochrome *c*, 1:100 (Neomarkers). Blots were washed in blocking solution and incubated with secondary antibodies: horseradish peroxidase (HRP)-conjugated goat anti-rabbit IgG (1:10,000) and HRP-conjugated goat anti-mouse IgG (1:10,000) (Jackson ImmunoResearch Laboratories) diluted in blocking solution. Secondary antibodies were detected using chemiluminescence (GE Healthcare).

Drosophila primary neuron culture

Primary neuron culture from *Drosophila* larval brains was adapted from Egger *et al.* (2013). Third instar *Drosophila* larval brains expressing ANF::GFP via the motor neuron GAL4 driver OK371 were dissected in Schneider's medium (Lonza BioWhittaker) supplemented with 20% fetal bovine serum (Life Technologies), 5 μg/ml bovine insulin, and 1× antibiotic-antimycotic solution (Sigma-Aldrich). Dissected brains were incubated in 0.5 mg/ml collagenase solution at room temperature for 1 h, followed by three washes in supplemented Schneider's medium. To make cell suspensions for culture, digested brain tissue was pipetted up and down before plating on concanavalin A (0.5 mg/ml)-treated glass cover slips. Additional supplemented Schneider's medium was added to cover the surface of the culture wells, and cells were incubated at 25°C. Culture medium was replaced every 24 h.

Immunofluorescence

Wandering third instar larvae were dissected, fixed, and stained as described previously (Hurd and Saxton, 1996) with the following modifications. Dissection was in standard phosphate-buffered saline (PBS), fixed in 4% paraformaldehyde (PFA) for 15 min, then rinsed with three changes of 0.1% Triton X-100 in PBS (PBST), and incubated for 30 min in blocking solution (5% normal goat serum in PBST). The primary antibodies used were chicken anti-GFP (1:1000; Aves Labs), mouse anti-cysteine string protein (CSP) (1:500), and rat anti-ELAV (1:500; Developmental Studies Hybridoma Bank, University of Iowa). Goat anti-chicken Alexa Fluor 488 and anti-rat Alexa Fluor 594 secondaries were used at 1:1000 (Invitrogen, Carlsbad, CA). Stained larvae were mounted on slides in Fluoromount-G mounting medium (Affymetrix eBioscience). Imaging was done with a spinning disk confocal fluorescence microscope (Nikon/Perkin Elmer/Improvision Ultraview) equipped with a Hamamatsu C9100-50 EM charge-coupled device camera. Control and mutant preparations were fixed, stained, and imaged using identical procedures.

For staining of primary cultured neurons, culture medium was removed and cells were rinsed three times in 1× PBS. Cells were fixed

in 4% PFA for 5 min followed by three rinses in PBST (0.1% Tween in PBS) and then blocked in 5% normal goat serum (NGS) at room temperature for 1 h. Because the antibodies against Unc104 and Khc were both generated in rabbits, anti-KHC (Cytoskeleton) was directly labeled with CF568 (Mix-N-Stain CF568 antibody labeling kit; Biotium) and cells were stained with the two antibodies sequentially. First, cells were incubated for 2 h with rabbit anti-unc104 (1:500) (Pack-Chung *et al*., 2007), rinsed, incubated with Alexa Fluor 647 anti-rabbit secondary antibody (1:1000; Invitrogen, Carlsbad, CA), along with 4′,6-diamidino-2-phenylindole dihydrochloride (DAPI) to label cell nuclei (1:1000), and then rinsed extensively. Second, the cells were incubated with the CF546 conjugated anti-KHC. Washes between each antibody incubation were 10 min, 3× in PBST. Stained cells were mounted in VECTASHIELD Antifade Mounting Medium (Vector Laboratories), sealed with nail polish, and imaged on a DeltaVision OMX SR microscope (GE Healthcare).

Live imaging

Time-lapse imaging of GFP-loaded organelles in axons was done with living third instar larvae 4–5 d after egg lay. A larva was placed in an imaging chamber modified from Fuger *et al*. (2007), anesthetized by injecting 50 ul of chilled Desflurane (Baxter) into the chamber, and sealed. For each animal, segmental nerve 7 or 8, in segments A4–A5, was imaged through the ventral body wall with the spinning disk microscope using a 60× 1.4 Na objective (Nikon). Images of DCVs and mitochondria were collected at 2 frames/s and 1 frame/s, respectively, for at least 500 frames. After imaging, larvae were returned to normal culture medium. Data were analyzed only from larvae that survived the procedure and recovered crawling mobility. Although larvae can survive in the anesthesia chamber for hours, imaging was restricted to the initial 30 min to reduce the potential for transport variation from physiological stress.

Superresolution microscopy

Superresolution 3D structured illumination microscopy (SIM) images were acquired on a DeltaVision OMX SR (GE Healthcare) equipped with a 60× 1.42 NA PlanApo oil immersion lens (Olympus); 405-, 488-, 568-, and 640-nm solid state lasers; and sCMOS cameras (pco.edge). Image stacks with 0.125-µm-thick z-sections, and 15 images per optical slice (three angles and five phases) were acquired using immersion oil with a refractive index 1.516. Images were reconstructed using Wiener filter settings of 0.003 and optical transfer functions (OTFs) measured specifically for each channel with SoftWoRx 6.5.2 (GE Healthcare) to obtain superresolution images with a twofold increase in resolution both axially and laterally. Images from different color channels were registered using parameters generated from a gold grid registration slide (GE Healthcare) and SoftWoRx 6.5.2 (GE Healthcare).

Superresolution image analysis

Colocalization of anti-Khc, anti-Unc-104(Imac), and ANF::GFP-loaded DCVs was measured using the spot detection extension in Imaris Bitplane software (version 8). Full-width half-maximal intensity was used to estimate DCV diameter as 180 nm and kinesin-1 and kinesin-3 diameter as 150 nm. Using these values, spots were generated from the reconstructed 3D SIM images. The spots-to-spots colocalization function was then used to identify all kinesin-1 or kinesin-3 generated spots within a specified threshold distance of the DCV spots. Colocalization of kinesin-1 or kinesin-3 or both motors with DCVs was expressed as a percentage over all detected DCVs. The predicted probability of Khc and Unc-104 colocalization on a DCV was calculated by (Khc-DCV%) × (Unc-104-DCV%).

To analyze random colocalization frequencies, a single region of interest away from the nucleus was selected from each of six different cells (three different experiments). Within each ROI, first the number of distinct observed anti-Khc and anti-Unc-104 spots were counted. Then R was used to generate random distributions of the appropriate numbers of spots for each motor in each ROI. This was repeated 100 times for each ROI. The average percentages of the random spots that colocalized with DCVs in each ROI were then calculated over a range of threshold distances. Standard errors were calculated for average random colocalization percentages using a sample size at the level of number of ROIs ($n = 6$). The average observed real motor-DCV colocalization percentages were measured at the same threshold distances in the same ROIs, and SEs were calculated using $n = 6$ ROIs.

Flux, particle tracking, and statistics

To measure overall transport of ANF-GFP DCVs from time-lapse image series, a line was drawn perpendicular to one nerve and the number of particles passing that line in each direction was counted for 200 frames. The counts were divided by elapsed time to derive flux values (number of vesicles per minute). A Student's *t* test (unequal variance) was used to assess significant differences in flux between control and mutant genotypes. To quantify the amount of DCV flux in primary neuron cultures, the Difference Filter plug-in was used to measure the proportion of moving to static signal (minimum difference = 20, offset = 2) (Andrews *et al*., 2010).

Single organelle DCV tracking was done using ImageJ 1.38x (Schneider *et al*., 2012) with the Manual Tracker plug-in. Automated tracking was not effective due to the high density of DCVs in nerves. In pilot tests with data from tracking all organelles in many time-lapse series, we previously determined that a sample size of five particles in each direction from five animals (one nerve each) provides a robust statistical analysis that is not substantially changed by increased sample sizes (Pilling *et al*., 2006; Barkus *et al*., 2008). In the present study, five anterograde and five retrograde DCVs that moved and remained in the plane of focus across a substantial portion of the field of view were tracked per nerve in 7–10 animals per genotype. Position-time data were analyzed as described previously (Pilling *et al*., 2006). A run is defined as a period of continuous motion of at least 1 pixel/frame in one direction for a minimum of three frames. While most DCVs in control animals move persistently toward either the terminal or the cell body, they do occasionally reverse their directions of movement for short distances. A run in the primary direction for a particular DCV is a forward run, that is, an anterograde DCV in the anterograde direction or a retrograde DCV in the retrograde direction. Because DCV reverse runs were rare and brief, our analyses focused on forward runs. Pauses were also infrequent, especially for anterograde DCVs in controls, so runs that could be defined by pauses or reversals at beginning and end were rare. More often, run lengths began and/or ended at the limits of the field of view. Because of this, our measured run lengths for controls in Table 1 are underestimates. Individual run velocities were derived from run length divided by time. Duty cycle refers to the fraction of time a particle spent in runs or pauses over its total track. To determine whether a transport parameter was significantly different due to genotype and to avoid repeated measures, standard linear contrast analysis was used (Pilling *et al*., 2006). Logarithmic transformation of input parameters was carried out to approximate a normal distribution as determined on a q-q plot. Linear contrast analyses were used for both transformed and untransformed data and the results were similar. Due to unequal sample sizes and variances between the groups, post hoc tests

were carried out (Dunnett's T3 and Tamhane's T2). Parameters showing a genotype-by-larva contrast significance of <0.05 were accepted as significantly different. Statistical analysis was carried out using SPSS Version 18.0 (SPSS, Chicago).

ACKNOWLEDGMENTS

We thank the TRiP at Harvard Medical School (National Institutes of Health/National Institute of General Medical Sciences R01-GM084947) for providing transgenic RNAi fly stocks used in this study, Thomas Schwarz for sharing Imac antibody, the labs of Jeremy Sanford and Doug Kellogg for sharing expertise in cytoplasmic fractionation, and Susan Strome for sharing Andreas. This work was supported by funds from National Institutes of Health GM46295 (W.M.S.).

REFERENCES

Al-Bassam J, Cui Y, Klopfenstein D, Carragher BO, Vale RD, Milligan RA (2003). Distinct conformations of the kinesin Unc104 neck regulate a monomer to dimer motor transition. J Cell Biol 163, 743–753.

Andrews S, Gilley J, Coleman MP (2010). Difference tracker: ImageJ plugins for fully automated analysis of multiple axonal transport parameters. J Neurosci Methods 193, 281–287.

Barkus RV, Klyachko O, Horiuchi D, Dickson BJ, Saxton WM (2008). Identification of an axonal kinesin-3 motor for fast anterograde vesicle transport that facilitates retrograde transport of neuropeptides. Mol Biol Cell 19, 274–283.

Block SM, Goldstein LS, Schnapp BJ (1990). Bead movement by single kinesin molecules studied with optical tweezers. Nature 348, 348–352.

Brady ST, Pfister KK, Bloom GS (1990). A monoclonal antibody against kinesin inhibits both anterograde and retrograde fast axonal transport in squid axoplasm. Proc Natl Acad Sci USA 87, 1061–1065.

Brendza KM, Rose DJ, Gilbert SP, Saxton WM (1999). Lethal kinesin mutations reveal amino acids important for ATPase activation and structural coupling. J Biol Chem 274, 31506–31514.

Brown A, Li Y, Slaughter I, Black MM (1993). Composite microtubules of the axon: quantitative analysis of tyrosinated and acetylated tubulin along individual axonal microtubules. J Cell Sci 104 (Pt 2), 339–352.

Butowt R, von Bartheld CS (2007). Conventional kinesin-I motors participate in the anterograde axonal transport of neurotrophins in the visual system. J Neurosci Res 85, 2546–2556.

Cai D, McEwen DP, Martens JR, Meyhofer E, Verhey KJ (2009). Single molecule imaging reveals differences in microtubule track selection between kinesin motors. PLoS Biol 7, e1000216.

Crimella C, Baschirotto C, Arnoldi A, Tonelli A, Tenderini E, Airoldi G, Martinuzzi A, Trabacca A, Losito L, Scarlato M, *et al*. (2011). Mutations in the motor and stalk domains of KIF5A in spastic paraplegia type 10 and in axonal Charcot-Marie-Tooth type 2. Clin Genet 82, 157–164.

deCuevas M (1993). An Analysis of the Stalk of Drosophila Kinesin Heavy Chain. PhDThesis. Boston: Harvard University.

Dollar G, Struckhoff E, Michaud J, Cohen RS (2002). Rab11 polarization of the Drosophila oocyte: a novel link between membrane trafficking, microtubule organization, and oskar mRNA localization and translation. Development 129, 517–526.

Dompierre JP, Godin JD, Charrin BC, Cordelieres FP, King SJ, Humbert S, Saudou F (2007). Histone deacetylase 6 inhibition compensates for the transport deficit in Huntington's disease by increasing tubulin acetylation. J Neurosci 27, 3571–3583.

Egger B, van Giesen L, Moraru M, Sprecher SG (2013). In vitro imaging of primary neural cell culture from Drosophila. Nat Protoc 8, 958–965.

Encalada SE, Szpankowski L, Xia CH, Goldstein LS (2011). Stable kinesin and dynein assemblies drive the axonal transport of mammalian prion protein vesicles. Cell 144, 551–565.

Ewer J, De Vente J, Truman JW (1994). Neuropeptide induction of cyclic GMP increases in the insect CNS: resolution at the level of single identifiable neurons. J Neurosci 14, 7704–7712.

Fuger P, Behrends LB, Mertel S, Sigrist SJ, Rasse TM (2007). Live imaging of synapse development and measuring protein dynamics using two-color fluorescence recovery after photo-bleaching at Drosophila synapses. Nat Protoc 2, 3285–3298.

Gho M, McDonald K, Ganetzky B, Saxton WM (1992). Effects of kinesin mutations on neuronal functions. Science 258, 313–316.

Glater EE, Megeath LJ, Stowers RS, Schwarz TL (2006). Axonal transport of mitochondria requires milton to recruit kinesin heavy chain and is light chain independent. J Cell Biol 173, 545–557.

Goizet C, Boukhris A, Mundwiller E, Tallaksen C, Forlani S, Toutain A, Carriere N, Paquis V, Depienne C, Durr A, *et al*. (2009). Complicated forms of autosomal dominant hereditary spastic paraplegia are frequent in SPG10. Hum Mutat 30, E376–E385.

Goldstein AY, Wang X, Schwarz TL (2008). Axonal transport and the delivery of pre-synaptic components. Curr Opin Neurobiol 18, 495–503.

Goldstein LS (1991). The kinesin superfamily: tails of functional redundancy. Trends Cell Biol 1, 93–98.

Goldstein LS (2001). Molecular motors: from one motor many tails to one motor many tales. Trends Cell Biol 11, 477–482.

Guardia CM, Farias GG, Jia R, Pu J, Bonifacino JS (2016). BORC functions upstream of kinesins 1 and 3 to coordinate regional movement of lysosomes along different microtubule tracks. Cell Rep 17, 1950–1961.

Hall DH, Hedgecock EM (1991). Kinesin-related gene unc-104 is required for axonal transport of synaptic vesicles in C. elegans. Cell 65, 837–847.

Heidemann SR, Landers JM, Hamborg MA (1981). Polarity orientation of axonal microtubules. J Cell Biol 91, 661–665.

Hendricks AG, Perlson E, Ross JL, Schroeder HW 3rd, Tokito M, Holzbaur EL (2010). Motor coordination via a tug-of-war mechanism drives bidirectional vesicle transport. Curr Biol 20, 697–702.

Hodge JJ, Choi JC, O'Kane CJ, Griffith LC (2005). Shaw potassium channel genes in Drosophila. J Neurobiol 63, 235–254.

Howard J, Hudspeth AJ, Vale RD (1989). Movement of microtubules by single kinesin molecules. Nature 342, 154–158.

Hurd DD, Saxton WM (1996). Kinesin mutations cause motor neuron disease phenotypes by disrupting fast axonal transport in Drosophila. Genetics 144, 1075–1085.

Hurd DD, Stern M, Saxton WM (1996). Mutation of the axonal transport motor kinesin enhances paralytic and suppresses Shaker in Drosophila. Genetics 142, 195–204.

Janke C, Kneussel M (2010). Tubulin post-translational modifications: encoding functions on the neuronal microtubule cytoskeleton. Trends Neurosci 33, 362–372.

Jeppesen GM, Hoerber JK (2012). The mechanical properties of kinesin-1: a holistic approach. Biochem Soc Trans 40, 438–443.

Karcher RL, Deacon SW, Gelfand VI (2002). Motor-cargo interactions: the key to transport specificity. Trends Cell Biol 12, 21–27.

Karsai G, Pollak E, Wacker M, Vomel M, Selcho M, Berta G, Nachman RJ, Isaac RE, Molnar L, Wegener C (2013). Diverse in- and output polarities and high complexity of local synaptic and non-synaptic signaling within a chemically defined class of peptidergic Drosophila neurons. Front Neural Circuits 7, 127.

Kim T, Gondre-Lewis MC, Arnaoutova I, Loh YP (2006). Dense-core secretory granule biogenesis. Physiology (Bethesda, MD) 21, 124–133.

Klopfenstein DR, Tomishige M, Stuurman N, Vale RD (2002). Role of phosphatidylinositol(4,5)bisphosphate organization in membrane transport by the Unc104 kinesin motor. Cell 109, 347–358.

Kulkarni A, Khan Y, Ray K (2017). Heterotrimeric kinesin-2, together with kinesin-1, steers vesicular acetylcholinesterase movements toward the synapse. FASEB J 31, 965–974.

Lachmanovich E, Shvartsman DE, Malka Y, Botvin C, Henis YI, Weiss AM (2003). Co-localization analysis of complex formation among membrane proteins by computerized fluorescence microscopy: application to immunofluorescence co-patching studies. J Microsc 212, 122–131.

Ling SC, Fahrner PS, Greenough WT, Gelfand VI (2004). Transport of Drosophila fragile X mental retardation protein-containing ribonucleoprotein granules by kinesin-1 and cytoplasmic dynein. Proc Natl Acad Sci USA 101, 17428–17433.

Lo KY, Kuzmin A, Unger SM, Petersen JD, Silverman MA (2011). KIF1A is the primary anterograde motor protein required for the axonal transport of dense-core vesicles in cultured hippocampal neurons. Neurosci Lett 491, 168–173.

Maday S, Twelvetrees AE, Moughamian AJ, Holzbaur EL (2014). Axonal transport: cargo-specific mechanisms of motility and regulation. Neuron 84, 292–309.

Martin M, Iyadurai SJ, Gassman A, Gindhart JG Jr, Hays TS, Saxton WM (1999). Cytoplasmic dynein, the dynactin complex, and kinesin are interdependent and essential for fast axonal transport. Mol Biol Cell 10, 3717–3728.

Messitt TJ, Gagnon JA, Kreiling JA, Pratt CA, Yoon YJ, Mowry KL (2008). Multiple kinesin motors coordinate cytoplasmic RNA transport on

a subpopulation of microtubules in Xenopus oocytes. Dev Cell 15, 426–436.
Nangaku M, Sato-Yoshitake R, Okada Y, Noda Y, Takemura R, Yamazaki H, Hirokawa N (1994). KIF1B, a novel microtubule plus end-directed monomeric motor protein for transport of mitochondria. Cell 79, 1209–1220.
Norris SR, Soppina V, Dizaji AS, Schimert KI, Sept D, Cai D, Sivaramakrishnan S, Verhey KJ (2014). A method for multiprotein assembly in cells reveals independent action of kinesins in complex. J Cell Biol 207, 393–406.
O'Donnell KH, Chen CT, Wensink PC (1994). Insulating DNA directs ubiquitous transcription of the Drosophila melanogaster alpha 1-tubulin gene. Mol Cell Biol 14, 6398–6408.
Pack-Chung E, Kurshan PT, Dickman DK, Schwarz TL (2007). A Drosophila kinesin required for synaptic bouton formation and synaptic vesicle transport. Nat Neurosci 10, 980–989.
Park JH, Schroeder AJ, Helfrich-Forster C, Jackson FR, Ewer J (2003). Targeted ablation of CCAP neuropeptide-containing neurons of Drosophila causes specific defects in execution and circadian timing of ecdysis behavior. Development 130, 2645–2656.
Pilling AD, Horiuchi D, Lively CM, Saxton WM (2006). Kinesin-1 and Dynein are the primary motors for fast transport of mitochondria in Drosophila motor axons. Mol Biol Cell 17, 2057–2068.
Rao S, Lang C, Levitan ES, Deitcher DL (2001). Visualization of neuropeptide expression, transport, and exocytosis in Drosophila melanogaster. J Neurobiol 49, 159–172.
Roux KH, Strelets L, Brekke OH, Sandlie I, Michaelsen TE (1998). Comparisons of the ability of human IgG3 hinge mutants, IgM, IgE, and IgA2, to form small immune complexes: a role for flexibility and geometry. J Immunol 161, 4083–4090.
Santos JG, Vomel M, Struck R, Homberg U, Nassel DR, Wegener C (2007). Neuroarchitecture of peptidergic systems in the larval ventral ganglion of Drosophila melanogaster. PLoS One 2, e695.
Saxton WM, Hicks J, Goldstein LS, Raff EC (1991). Kinesin heavy chain is essential for viability and neuromuscular functions in Drosophila, but mutants show no defects in mitosis. Cell 64, 1093–1102.
Saxton WM, Hollenbeck PJ (2012). The axonal transport of mitochondria. J Cell Sci 125, 2095–2104.
Schneider CA, Rasband WS, Eliceiri KW (2012). NIH Image to ImageJ: 25 years of image analysis. Nat Methods 9, 671–675.
Snow JJ, Ou G, Gunnarson AL, Walker MR, Zhou HM, Brust-Mascher I, Scholey JM (2004). Two anterograde intraflagellar transport motors cooperate to build sensory cilia on C. elegans neurons. Nat Cell Biol 6, 1109–1113.
Stone MC, Roegiers F, Rolls MM (2008). Microtubules have opposite orientation in axons and dendrites of Drosophila neurons. Mol Biol Cell 19, 4122–4129.
Stowers RS, Megeath LJ, Gorska-Andrzejak J, Meinertzhagen IA, Schwarz TL (2002). Axonal transport of mitochondria to synapses depends on milton, a novel Drosophila protein. Neuron 36, 1063–1077.
Tomishige M, Klopfenstein DR, Vale RD (2002). Conversion of Unc104/KIF1A kinesin into a processive motor after dimerization. Science 297, 2263–2267.
Uchida A, Alami NH, Brown A (2009). Tight functional coupling of kinesin-1A and dynein motors in the bidirectional transport of neurofilaments. Mol Biol Cell 20, 4997–5006.
Vale RD (2003). The molecular motor toolbox for intracellular transport. Cell 112, 467–480.
Vomel M, Wegener C (2007). Neurotransmitter-induced changes in the intracellular calcium concentration suggest a differential central modulation of CCAP neuron subsets in Drosophila. Dev Neurobiol 67, 792–808.
Zahn TR, Angleson JK, MacMorris MA, Domke E, Hutton JF, Schwartz C, Hutton JC (2004). Dense core vesicle dynamics in Caenorhabditis elegans neurons and the role of kinesin UNC-104. Traffic 5, 544–559.